Optimal sizing of battery energy storage system in smart microgrid considering virtual energy storage system and high photovoltaic penetration

Changhong Xie [a], Dongxiao Wang [a,b], Chun Sing Lai [a,c,*], Runji Wu [a], Xiaomei Wu [a], Loi Lei Lai [a]

[a] Department of Electrical Engineering, School of Automation, Guangdong University of Technology, Guangzhou, 510006, China

[b] Australia Energy Market Operator, Melbourne, 3000, Australia

[c] Brunel Institute of Power Systems, Department of Electronic & Electrical Engineering, Brunel University London, London UB8 3PH, UK

[*] Corresponding author: chunsing.lai@brunel.ac.uk

ABSTRACT: In the smart microgrid system, the optimal sizing of battery energy storage system (BESS) considering virtual energy storage system (VESS) can minimize system cost and keep system stable operation. This paper proposes a two-layer BESS optimal sizing strategy considering dispatch of VESS in a smart microgrid with high photovoltaic (PV) penetration. In the first layer, VESS modelling and aggregation are established, and the initial size of BESS is determined by considering VESS participation in demand response program. In the second layer, the optimal sizing of BESS is studied and the optimal energy resources dispatching strategy is formulated via considering various constraints in the system. The mean-variance Markowitz theory is applied to assess the risk of system cost variability due to the presence of PV and load uncertainties. With the ratio of load varies from 70% to 130%, and PV generation ratio from 40% to 100%, sensitivity analysis reveals the optimal size of BESS is less impacted by PV generation change. Also with VaR(95%) the risk of system cost variability can be further reduced through VESS participation.

Keywords— Battery energy storage system, High photovoltaic penetration, Optimal sizing, Risk control, Virtual energy storage system (VESS)

Nomenclature

Abbreviations	
BESS	Battery energy storage system
CES	Community energy storage
DE	Differential evolution algorithm
EMS	Energy management system
HES	Home energy storage
MILP	Mixed-integer linear programming
MINLP	Mixed-integer nonlinear programming
PV	Photovoltaic
VSOC	VESS State of charge
BSOC	BESS State of charge
VaR	Value at risk
VESS	Virtual energy storage system
Indices	

i	Index for the household
s	Index for the scenario
t	Index for the time slot
T	Index for the year
Parameters	
A_{BESS}^{E}	The BESS per unit capacity cost in \$/kWh
A_{BESS}^{P}	The BESS per unit power cost in \$/kW
$A_{BESS\_M}^{E}$	The maintenance cost of BESS unit capacity in \$/kWh
$A_{BESS\_M}^{P}$	The maintenance cost of BESS unit power in \$/kW
A_{PV}	The size of PV in m^2
cop	The air conditioning performance parameters
C_a	The heat capacity value of indoor air in $\mathrm{J}/(\mathrm{kg}\cdot°\mathrm{C})$
C_w	The heat capacity value of walls in $\mathrm{J}/(\mathrm{kg}\cdot°\mathrm{C})$
$C_{buy}(t)$	The price of electricity purchasing from the distribution network to microgrid at time t in \$/kWh
$C_{sell}(t)$	The price of electricity selling from microgrid to the distribution network at time t in \$/kWh
E_{VES_Mi}	The rated capacity of VESS of the i^{th} building in kWh
E_{VES_M}	The rated capacity of VESS for the VESS aggregator in kWh
I_{PVO}	The average solar irradiation on the PV array at the nominal operating cell temperature in $\mathrm{kWh/m^2}$
K_{coef}	The present value factor
M_a	The mass value of indoor air in kg
M_w	The mass value of walls in kg
N	The number of the time slot
M	The number of air conditioning households in the aggregator
N_{st}	The standardization factor
P_{ac}	The value of air conditioning rated power in kW
$P_{\max}$	The maximum value of power exchange in kW
$P_{PV}^{\max}$	The upper limit of PV generation power in kW
$P_{BESS,Chr}^{\min}$	The lower limit value of charging power for BESS in kW
$P_{BESS,Chr}^{\max}$	The upper limit value of charging power for BESS in kW
$P_{BESS,Dis}^{\min}$	The lower limit value of discharging power for BESS in kW

$P_{BESS,Dis}^{\max}$	The upper limit value of discharging power for BESS in kW
$P_{Load}(t)$	The microgrid total load at time t in kW
$P_{Uncontro\_load}(t)$	The constant load of the microgrid (considered to be all loads except the aggregated air conditioning load) at time t in kW
R_B	The geometric ratio of the irradiance incident on the tilted plane and the horizontal plane
R_{eq}	The wall equivalent thermal resistance in $(\mathrm{m}^2 \cdot ^\circ\mathrm{C})/\mathrm{W}$
R_{wr}	The external wall and ambient air thermal resistance in $(\mathrm{m}^2 \cdot ^\circ\mathrm{C})/\mathrm{W}$
R_{wa}	The internal wall and indoor air thermal resistance in $(\mathrm{m}^2 \cdot ^\circ\mathrm{C})/\mathrm{W}$
r	The discount factor
r'	The equivalent discount factor
S	The number of represent scenarios
$BSOC^{\min}$	The lower limit value of BSOC for BESS
$BSOC^{\max}$	The upper limit value of BSOC for BESS
T_{ref}	The reference cell temperature for PV array, set as 25 °C
T_{CO}	The cell temperature for PV array at the nominal operation cell temperature in °C
T_{AO}	The ambient temperature for PV at the nominal operation cell temperature in °C
T_{life}	The BESS's life in years
$T_r^{\min}$	Lower limit value of indoor thermal comfort temperature in °C
$T_r^{\max}$	Upper limit value of indoor thermal comfort temperature in °C
$T_w^{\min}$	Lower limit value of required building wall temperature in °C
$T_w^{\max}$	Upper limit value of required building wall temperature in °C
$T_{amb}(t)$	The temperature value for ambient at time t in °C
α	The alpha distribution parameter
β	The beta distribution parameter
β_{tc}	The temperature coefficient
δ_{self_d}	The self-discharging rate for BESS
$\eta_{BESS,Chr}$	The charging efficiency of BESS
$\eta_{BESS,Dis}$	The discharging efficiency of BESS
η_{PV}	The actual efficiency of the PV generation
η_{ref}	The PV generator efficiency at reference cell temperature
λ	The indoor heat gain in $\mathrm{W/m}^2$

γ	Scale factor
ζ	The conversion factor of J to kWh
τ	The time slot in hour
μ	The mean of the load forecast error
σ_l^2	The variance of the load forecast error
ΔL	The load forecast error
ΔP	The prediction error of photovoltaic output
Variables	
C_{BESS}	The investment cost of BESS in $
$C_{O\&M}$	The operation cost of BESS in $
C_{Init}	The minimum operation cost of microgrid in $
C_O	The intra-day operation cost of microgrid system in $
C_M	The annual maintenance cost of BESS in $
C_{BESS_back}	The net profit of BESS in $
$C_{arbi}(t)$	The arbitrage of electricity price fluctuation at time *t* in $
$E_{BESS,Init}^{rate}$	The BESS initial rated capacity in kWh
E_{BESS}^{rate}	The BESS rated capacity in kWh
$E_{BESS}(t)$	The capacity for BESS at time *t* in kWh
$E_{VES\_i}(t)$	The capacity of VESS of the i^{th} building at time *t* in kWh
$E_{VES}(t)$	The capacity for the VESS aggregator at time *t* in kWh
$I_B(t)$	The global irradiation on the array at time *t* in kW/m^2
$I_D(t)$	The diffuse irradiation on the array at time *t* in kW/m^2
$I_{PV}(t)$	The solar irradiation incident on the array at time *t* in kW/m^2
$\min C$	The minimum system cost in $
$P_{BESS,Init}^{rate}$	The BESS initial rated power in kW
P_{BESS}^{rate}	The BESS rated power in kW
$P_{BESS,\max}^{rate}$	The maximum possible rated power of BESS in kW
$P_{PV}(t)$	The photovoltaic output power at time *t* in kW
$P_{BESS,Chr}(t+1)$	The charge power of BESS at time *t*+1 in kW
$P_{BESS,Dis}(t+1)$	The discharging power of BESS at time *t*+1 in kW
$P_{VES\_i}(t)$	The power of VESS of the i^{th} building at time *t* in kW

$P_{VES}(t)$	The power for the VESS aggregator at time *t* in kW
$P_{buy}(t)$	The amount of power purchased from the distribution network at time *t* in kW
$P_{sell}(t)$	The amount of power selling to the distribution network at time *t* in kW
$Q_{ex\_a\_r}(t)$	The heat exchange between indoor air and ambient air at time *t*
$Q_{ex\_Iw\_r}(t)$	The heat exchange between inner wall and indoor air at time *t*
$Q_{ac}(t)$	The cooling capacity of air conditioning at time *t*
Q_{gain}	The indoor heat gain
$Q_{ex\_Ow\_a}(t)$	The heat exchange between outer wall and ambient air at time *t*
$S_{ac}(t)$	The switch state of the air conditioning at time *t*
$BSOC(t)$	State of charge for BESS at time *t*
$VSOC(t)$	The state of charge for the VESS aggregator at time *t*
$T_r(t)$	The temperature value for indoor air at time *t* in °C
$T_w(t)$	The temperature value for building wall at time *t* in °C
$T_A(t)$	The ambient temperature for PV at time *t* in °C
$x_{buy}(t)$	The selling electricity status for microgrid at time *t*, 1 shows the microgrid system buys electricity from the distribution network, 0 does not
$x_{sell}(t)$	The purchasing electricity status for microgrid at time *t*, 1 shows the microgrid system sells electricity power to the distribution network, 0 does not
δ_1	The increment of rated capacity for BESS in kWh
δ_2	The increment of rated power for BESS in kW
$\mu_{BESS,Chr}(t)$	The charging status of BESS at time *t*, 1 means BESS is charging, 0 means not charging
$\mu_{BESS,Dis}(t)$	The discharging status of BESS at time *t*, 1 means BESS is discharging, 0 means not discharging

1. Introduction

With the global fossil fuel shortage and the increasing concerns for the environment, the photovoltaic (PV) power penetration has been rapidly developing in recent decades. According to the report of the International Renewable Energy Agency, photovoltaic power generation is currently the fastest growing distributed energy source and will account for 22% of the overall global power generation by 2050 [1]. However, due to the uncertainty of photovoltaic power generation, high photovoltaic penetration makes the power grid face many challenges [2], such as reverse power flow, voltage fluctuations, frequency fluctuations and harmonics. Therefore, the penetration of photovoltaic power generation has been curtailed to some extent to keep the stability of the grid. On the other hand, battery energy storage system (BESS) can well alleviate the uncertainty of renewable resources and increase large-scale PV penetration level [3-4]. BESS is playing a vital role to improve energy efficiency and keep the system stable operation in the future power grid [5]. Currently, although the cost of energy storage has

gradually decreased and lithium-ion battery technology has developed more maturely [4], the high cost of the battery is still limiting the rapid construction of BESS [6]. To reduce BESS investment cost and lower the burden of the system operator, the size of BESS needs to be optimized while meeting various system constraints.

A large number of researches has presented various optimal sizing strategy of BESS. Based on the subsidies of PV, electricity price mechanisms, and uncertainties of PV and load, Zhou et al. proposed an optimal sizing strategy of PV and BESS in a smart household [7]. Liu et al. provided the optimal sizing strategy, where a two-layer hybrid energy storage system is established to meet different power load with the various response time [8]. Considering a series of different cost, technology and environment, an optimal strategy was given in [9] to optimize the placement, sizing and dispatching of BESS. Hemmati et al. presented the optimal sizing strategy of BESS considering PV and load uncertainties, and the stochastic mix integer nonlinear programming was solved by Monte Carlo simulation and advanced adaptive particle swarm optimization [10]. The reverse power flow due to the high PV penetration was coped by BESS in [11], and an optimal sizing method of BESS was proposed aiming to minimize the system cost. In order to minimize the levelized cost of energy and imbalance between power supply and demand in the system, Lai et al. carried out an optimal sizing of PV and energy storage system [12]. To reduce the wind power forecast error, a sizing method of ESS was presented by probabilistic method in [13]. Ban et al. proposed an optimal sizing method of PV and BESS in nanogrid to serve the battery swapping station of electric vehicles considering the investment cost of BESS, the characteristics of the swapping station and uncertainties [14]. In addition, the economic feasibility was analyzed in the size optimization of centralized BESS and distributed BESS in [15-17]. The results in [15] showed that the centralized community with BESS can help end-users reduce BESS investment cost. Distributed users can get the maximum net present value benefit if they own BESS independently. Considering different ratios of battery storage and thermal storage, Terlouw et al. comparatively studied home energy storage (HES) and community energy storage (CES) considering the operation costs and environment [16]. The results showed CES is superior to HES in economic and environmental aspects. In [17], Stelt et al. provided energy storage system's investment costs in per kilowatt-hour, which are crucial for the economic feasibility of HES and CES. Zhong et al. introduced shared BESS to reduce system cost, which utilized integrated BESS by the operator instead of individual BESS [18].

It can be observed from the literature review that the system cost is taken as the main index considering various factors in the research of BESS optimal sizing. However, few researches have optimized the size of BESS to minimize system cost under high photovoltaic penetration whilst the risk of system cost variability is assessed. Consequently, it has a negative impact on ensuring the reliability of the system with the increasing penetration of solar photovoltaic energy, when the risk of system cost variability is neglected.

On the other hand, demand response technology provides new directions for system cost minimization with the development of smart grid technology. Households and office buildings have high power consumption [2], where controllable load (such as air conditioner and heat pumps) accounts for a large part. Through demand response strategies, thermal controllable load can be well utilized to reduce energy cost. Given that air conditioners have relatively fast response time with least end-user disruptions [19] and consume large amount of energy, air-conditioned buildings can be pre-cooled or pre-heated to provide energy buffer and form the virtual energy storage system (VESS). VESSs have a great potential in lowering system peak demand through demand response strategies, reducing system operator investment cost and benefiting end-users. It should also be noted that the building sector provides great potential in cost effective emission mitigation and economic gains with existing technologies and policies. Ma et al. revealed the building carbon emissions have a significant impact on emission peak, and the low carbon roadmap was further developed about residential buildings [20]. Furthermore,

in the field of the decoupling of per capita carbon dioxide emission from the human development index, Chen et al. [21] pointed out the fundamental reason for strengthening decoupling effect is the reduction of carbon dioxide emissions. Therefore, to further promote the emission reduction for building sector, it is necessary to insist on implementing energy saving and emission-reduction strategy [22].

Currently, there have been some researches on VESSs. The round-trip efficiency of VESS was analyzed in [23]. Considering the building's heat storage characteristics [24], VESS was used for energy dispatching to reduce operation costs [25], and the results in [26] demonstrated that the energy dispatching of VESS relied on building parameters and the occupancy time etc. Further, Zhu et al. improved the stability of regional integrated energy system and reduced system cost by joint VESS (i.e. combining electric vehicle energy storage and air conditioning thermal energy storage) [27]. In addition, the VESS formed by refrigerators [28] and heating ventilation and air conditioning [29] was applied to frequency service for power system. However, to the best of the authors' knowledge, no previous research has taken into account the accurate modelling of VESS in BESS optimal sizing strategy, which means that the system overall cost may be further reduced with VESS participation.

To close the research gap as mentioned above, this paper proposes a two-layer optimal sizing strategy for the battery energy storage system considering the dispatch of virtual energy storage systems and high PV penetration. The distinguished features of this paper are summarized as follows:

(1) An accurate VESS model is formulated, and further aggregated to participate system dispatch and control.

(2) A two-layer BESS optimal sizing strategy is proposed considering various system constraints. System operation cost is minimized via optimally dispatching the photovoltaic system, battery energy storage system and virtual energy storage system.

(3) A risk component is introduced in the control objective based on the mean-variance Markowitz theory. The risk-based decision-making fully considers the impacts from system uncertainties which greatly influences system dispatch results.

The remaining parts of the paper are as follows. The problem description is introduced in Section 2. Section 3 presents the system components modelling. In Section 4, the mathematical model for the proposed strategy is provided. The implementation of BESS optimal sizing strategy is described in Section 5. In Section 6, case studies are carried out and simulation results are analyzed to demonstrate the effectiveness of the proposed strategy. Conclusions are given in Section 7.

2. Problem Description

The scope of this paper is to investigate the optimal sizing of BESS considering VESS and high PV penetration in the system and the corresponding optimal energy dispatch of smart microgrid system resources from the operator perspective.

As shown in Fig. 1, smart microgrid system is a new type of grid composed by photovoltaic power generation system, battery energy storage system, microgrid power load, energy management system (EMS) and various distribution infrastructures. In this paper, the microgrid system operator owns the battery energy system and the photovoltaic system, which can reduce the investment cost for end-users [15]. The photovoltaic power generation system provides users with renewable electricity. BESS consumes the surplus photovoltaic power whilst ensuring the power quality of the microgrid system. The smart microgrid system is connected to the power distribution network, which can work in both islanded modes and grid-connected modes. In the system, air-conditioned households are aggregated and controlled by an aggregator to form the virtual energy storage system [30], and

the end-users are regulated by the aggregator without compromising their thermal comfort. EMS can optimally dispatch power resources and manage the energy balance of the microgrid [31].

Under the time-of-use electricity price mechanism, the microgrid system operator has two objectives: 1) making full use of the battery energy storage system and the virtual energy storage system to increase photovoltaic penetration rate; and 2) minimizing the microgrid system cost including investment cost and system operation cost through BESS optimal sizing strategy. It should be noted that the investment cost mainly refers to the construction cost of the system equipped with the battery energy storage system, and the system operation cost is the cost of purchasing electricity from the distribution network and the maintenance cost of the system.

In the proposed two-layer optimal sizing framework, a more accurate two-parameter thermal model is established to aggregate and quantify the virtual energy storage system. In the first layer, the initial size of BESS is determined by mixed integer linear programming considering dispatch of VESS to reduce the energy cost. In the second layer, the differential evolution algorithm and the iterative search method are applied to find the optimal size of BESS, further determining the optimal energy resources dispatch including PV system, VESS and BESS. In addition, the mean-variance Markowitz theory is adopted to assess the risk of system cost variability considering uncertainties of PV generation and load.

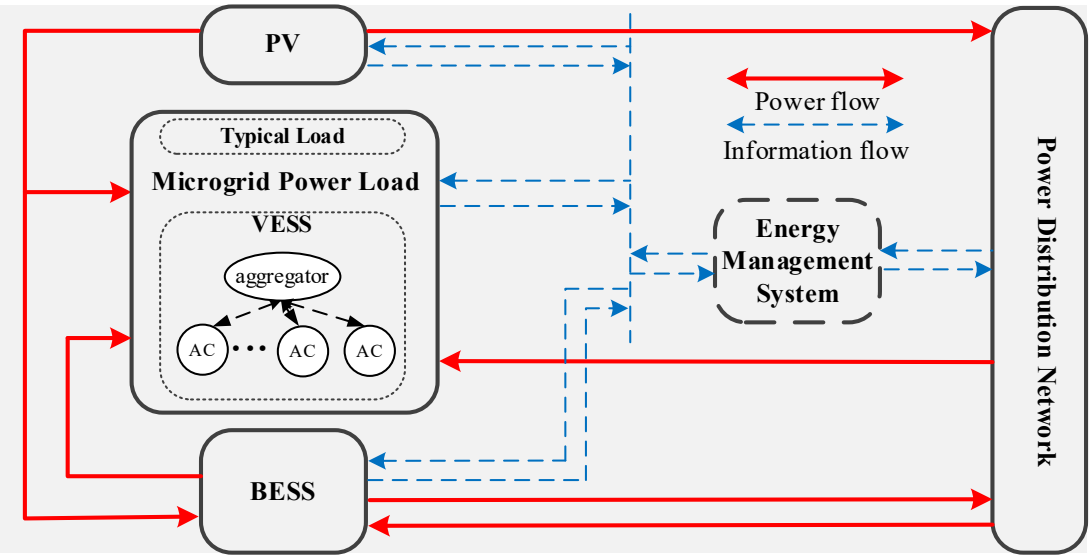

Fig. 1. Smart microgrid system.

3. System Components Modelling

In this section, the modelling of various components in this paper is introduced, which includes modelling of VESS, BESS and PV generation. In the last subsection, the uncertainties of PV generation and load are given.

3.1. VESS modelling

Previous researchers have developed different complexities of thermal models to represent the thermal process of air-conditioned households [32]. However, the thermal model of air-conditioned household is built through the first order differential equations [33], which cannot reflect the precise thermal dynamic process of air-conditioned households owing to the inherent large thermal mass temperature dynamics. Therefore, a more accurate two-parameter thermal model has been established in [34] to simulate the indoor thermal change process of air-conditioned households, but these studies did not take into account the heat output (heat gain) such as household machinery and people [35]. Based on previous work, this paper innovatively proposes to add the heat

gain parameters [36] into the two-parameter thermal model to more accurately capture the thermal process. Thermal process of a single air-conditioned household is shown in Fig. 2. The thermodynamic process of a single air-conditioned household can be described as follows [34]:

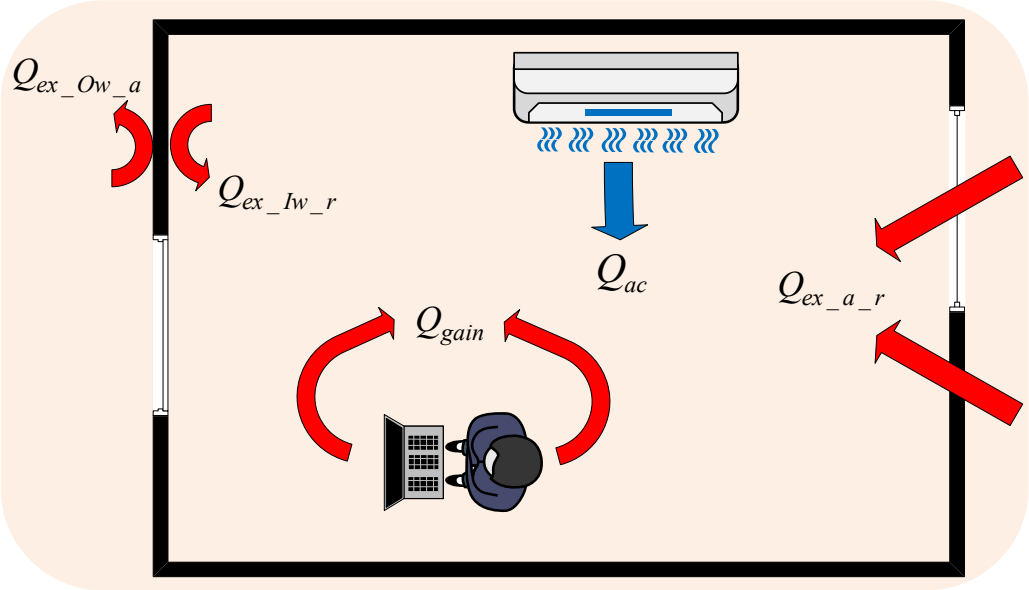

Fig. 2. Indoor thermal process.

$$\frac{dT_r(t)}{dt} = \frac{1}{M_a \cdot C_a}\left[\frac{dQ_{ex\_a\_r}(t)}{dt} + \frac{dQ_{ex\_Iw\_r}(t)}{dt} + \frac{dQ_{gain}}{dt} - \frac{dQ_{ac}(t)}{dt}\right] \tag{1}$$

$$\frac{dT_w(t)}{dt} = \frac{1}{M_w \cdot C_w}\left[\frac{dQ_{ex\_Ow\_a}(t)}{dt} + \frac{dQ_{ex\_Iw\_r}(t)}{dt}\right] \tag{2}$$

$$\frac{dQ_{ex\_a\_r}(t)}{dt} = \frac{T_{amb} - T_r}{R_{eq}} \tag{3}$$

$$\frac{dQ_{ex\_Iw\_r}(t)}{dt} = \frac{T_w - T_r}{R_{wr}} \tag{4}$$

$$\frac{dQ_{ac}(t)}{dt} = cop \cdot P_{ac} \tag{5}$$

$$\frac{dQ_{gain}}{dt} = \lambda \tag{6}$$

$$\frac{dQ_{ex\_Ow\_a}(t)}{dt} = \frac{T_{amb} - T_w}{R_{wa}} \tag{7}$$

Equations (1) - (2) represent the rate of change of indoor air temperature and wall temperature respectively; Equations (3) - (7) represent the heat exchange between indoor air and ambient air, the heat exchange between inner wall and indoor air, the cooling capacity of air conditioning, indoor heat gain, and the heat exchange between outer wall and ambient air respectively. Noted that relevant parameters for the household can be calculated by the physical data [37].

To conveniently calculate indoor air temperature and build a flexible dispatch scheme, the proposed dynamic thermal model can be linearized as [34]:

$$T_r(t) = T_r(t-1) + \frac{1}{M_a \cdot C_a} \cdot \left[\frac{T_{amb}(t-1) - T_r(t-1)}{R_{eq}} + \frac{T_w(t-1) - T_r(t-1)}{R_{wr}} + \lambda - cop \cdot P_{ac} \cdot S_{ac}(t-1) \right] \cdot \tau \quad (8)$$

$$t \in [1, N]$$

$$T_w(t) = T_w(t-1) + \frac{1}{M_w \cdot C_w} \cdot \left[\frac{T_{amb}(t-1) - T_w(t-1)}{R_{wa}} + \frac{T_r(t-1) - T_w(t-1)}{R_{wr}} \right] \cdot \tau, \quad t \in [1, N] \quad (9)$$

Where, the whole day (24 hours) is equally divided into *N* segments, and the interval of each segment is τ. It should be noted that the switch state of the air conditioner in this paper is considered as a binary variable, 1 is ON and 0 is OFF; and the switch state of the air conditioner is determined by the comfort temperature range set by the user:

$$T_r^{\min} \le T_r(t) \le T_r^{\max} \quad (10)$$

$$T_w^{\min} \le T_w(t) \le T_w^{\max} \quad (11)$$

$$S_{ac}(t) = \begin{cases} 1, & ON \\ 0, & OFF \end{cases} \quad (12)$$

The unique thermal inertia of air-conditioned households can be used to aggregate the air-conditioned households to form a virtual energy storage system similar to the traditional energy storage system. Taking summer as an example, in order to meet the users' thermal comfort, the air conditioner is turned on for cooling, and the household indoor temperature drops slowly. In this situation, the virtual energy storage system is considered in the charging state. When the air conditioner is turned off, the indoor temperature of the household rises slowly, and the VESS is considered in the discharging state. Therefore, the capacity of a single household's virtual energy storage system is expressed as follows:

$$E_{VES\_Mi} = M_{a\_i} \cdot C_{a\_i} \cdot (T_{r\_i}^{\max} - T_{r\_i}^{\min}) \cdot \zeta \quad (13)$$

$$E_{VES\_i}(t) = M_{a\_i} \cdot C_{a\_i} \cdot (T_{r\_i}^{\max} - T_{r\_i}(t)) \cdot \zeta \quad (14)$$

Equation (8) is substituted into Equation (14) to obtain:

$$E_{VES\_i}(t+1) = E_{VES\_i}(t) + P_{VES\_i}(t) \cdot \tau \quad (15)$$

$$P_{VES\_i}(t) = \frac{\zeta}{\tau} \cdot \left[\frac{R_{eq\_i} + R_{wr\_i}}{R_{eq\_i} \cdot R_{wr\_i}} \cdot T_{r\_i}(t) - \frac{1}{R_{wr\_i}} \cdot T_{w\_i}(t) - \frac{1}{R_{eq\_i}} \cdot T_{amb\_i}(t) - \lambda_i + S_{ac\_i}(t) \cdot Q_{ac\_i}(t) \right] \quad (16)$$

To meet the capacity requirements of participating demand response programs, VESSs are further aggregated and the aggregated capacity/power are denoted as:

$$E_{VES\_M} = \zeta \cdot \sum_{i=1}^{M} \left[M_{a\_i} \cdot C_{a\_i} \cdot (T_{r\_i}^{\max} - T_{r\_i}^{\min}) \right] \quad (17)$$

$$E_{VES}(t+1) = E_{VES}(t) + P_{VES}(t) \cdot \tau \quad (18)$$

$$E_{VES}(t) = \zeta \cdot \sum_{i=1}^{M} \left[M_{a\_i} \cdot C_{a\_i} \cdot (T_{r\_i}^{\max} - T_{r\_i}(t)) \right] \quad (19)$$

$$P_{VES}(t) = \frac{\zeta}{\tau} \cdot \sum_{i=1}^{M} \left[\frac{R_{eq\_i} + R_{wr\_i}}{R_{eq\_i} \cdot R_{wr\_i}} \cdot T_{r\_i}(t) - \frac{1}{R_{wr\_i}} \cdot T_{w\_i}(t) - \frac{1}{R_{eq\_i}} \cdot T_{amb\_i}(t) - \lambda_i + S_{ac\_i}(t) \cdot Q_{ac\_i}(t) \right] \quad (20)$$

$$VSOC(t) = \frac{E_{VES}(t)}{E_{VES\_M}} \cdot 100\% \quad (21)$$

3.2. BESS modelling

The BESS model takes into account the charging and discharging power, self-discharging rate [15], and charging and discharging efficiency of the battery energy storage system [38], as descripted below:

$$E_{BESS}(t+1) = E_{BESS}(t) \cdot (1-\delta_{self\_d}) + P_{BESS,Chr}(t+1) \cdot \tau \cdot \eta_{BESS,Chr} - P_{BESS,Dis}(t+1) \cdot \tau / \eta_{BESS,Dis} \quad (22)$$

$$BSOC(t) = \frac{E_{BESS}(t)}{E_{BESS}^{rate}} \cdot 100\% \quad (23)$$

$$E_{BESS}(t) = E_{BESS,Init}, \quad if \ t = 1 \quad (24)$$

$$P_{BESS,Chr}^{\min} \le P_{BESS,Chr}(t) \le P_{BESS,Chr}^{\max} \quad (25)$$

$$P_{BESS,Dis}^{\min} \le P_{BESS,Dis}(t) \le P_{BESS,Dis}^{\max} \quad (26)$$

$$BSOC^{\min} \le BSOC(t) \le BSOC^{\max} \quad (27)$$

Equations (25) - (27) represent the charging/discharging power constraint and the state of charge constraint of BESS.

3.3. PV modelling

Photovoltaic output power is mainly influenced by the size of PV farm, available solar irradiance and ambient temperatures. According to [39], the model of PV power generation can be formulated as:

$$P_{PV}(t) = A_{PV} \cdot I_{PV}(t) \cdot \eta_{PV} \quad (28)$$

$$I_{PV}(t) = (I_B(t) + I_D(t)) \cdot R_B + I_D(t) \quad (29)$$

$$\eta_{PV} = \eta_{ref} \cdot \left[1 - \frac{0.9 \cdot \beta_{tc} \cdot I_{PV}(t)}{I_{PVO}} \cdot (T_{CO} - T_{AO}) - \beta_{tc} \cdot \left(T_A(t) - T_{ref} \right) \right] \quad (30)$$

It can be observed that the photovoltaic output power mainly depends on the solar irradiation incident and the ambient temperature at time *t*, which varies with time and causes PV generation uncertainty.

3.4. Uncertainties of PV power generation and load demand

In this paper, PV power generation and load demand are regarded as system uncertainties. The historical data in day-ahead market are used as correlated scenarios, hence allowing the correlated probability distributions to be estimated based on the statistical correlations among these uncertainties. Time-series-based methods, such as autoregressive integrated moving average model, are adopted in this work to generate correlated scenarios [40]. The forecast errors are handled by the different probability distribution functions. According to [41], Beta distribution and Gaussian distribution can be adopted to model PV prediction error and load forecast error respectively. The PV prediction error is discussed as:

$$f_{PV}(\Delta P; \alpha, \beta) = (\Delta P)^{\alpha-1} \cdot (1-\Delta P)^{\beta-1} \cdot N_{st} \quad (31)$$

The load forecast error is discussed as:

$$f(\Delta L; \mu, \sigma_l^2) = \frac{1}{\sqrt{2\pi\sigma_l^2}} \exp\left[-\frac{(\Delta L - \mu)}{2\sigma_l^2} \right] \quad (32)$$

4. Mathematical Model for the Proposed Strategy

In this section, a two-layer BESS optimal sizing strategy is proposed to minimize system cost considering the involvement of VESS in smart microgrid with high photovoltaic penetration.

In the first layer, with minimizing the operation cost of microgrid and maximizing the on-site consumption of PV generation as the objective, the initial size of BESS is determined by considering VESS participation in demand response program, which can reduce the computational burden of the iterative algorithm. In the second layer, the optimal sizing of BESS is developed and the optimal energy resources dispatching strategy is formulated via considering various constraints in the system. In addition, the mean-variance Markowitz theory is applied to assess the risk of system cost variability which is caused by uncertainties of PV generation and load. The objective in this layer is to minimize system investment cost and operation cost in a risk-hedging manner. The detailed mathematical model will be given in the following subsections.

4.1. First layer-BESS initial sizing model

4.1.1 Objective

In this layer, considering VESS participation in demand response program, a mixed-integer linear programming (MILP) model is proposed to minimize the operation cost of microgrid, and the initial size of BESS is developed subsequently to achieve the on-site consumption of photovoltaics in the microgrid. The model is formulated as follows:

$$C_{Init} = \min \sum_{t=1}^{N} \left(P_{buy}(t) \cdot C_{buy}(t) - P_{sell}(t) \cdot C_{sell}(t) \right) \cdot \tau \tag{33}$$

The relevant variables in Equation (33) are further given as:

$$\begin{cases} P_{sell}(t) = P_{PV}(t) - P_{Load}(t), & P_{PV}(t) > P_{Load}(t) \\ P_{buy}(t) = P_{Load}(t) - P_{PV}(t), & P_{PV}(t) < P_{Load}(t) \end{cases} \tag{34}$$

$$P_{Load}(t) = P_{Uncontro\_load}(t) + \sum_{i=1}^{M} P_{ac\_i}(t) \cdot S_{ac\_i}(t) \tag{35}$$

The initial size of BESS is formulated as follows:

$$P_{BESS,Init}^{rate} = \max\left(P_{PV}(t) - P_{Load}(t) \right) \tag{36}$$

$$E_{BESS,Init}^{rate} = \frac{\sum_{t=1}^{N} \left[P_{PV}(t) - P_{Load}(t) + \left| P_{PV}(t) - P_{Load}(t) \right| \right] \cdot \tau}{2 \cdot \eta_{BESS,Chr}} \tag{37}$$

$$P_{BESS,\max}^{rate} = \max(P_{Load}(t)) \tag{38}$$

4.1.2 Constraints

To ensure stable operation of the system, the following constraints should be met:

1) Constraints of power balance

The electrical network must meet the supply and demand balance to keep system stable operation, as shown in Equation (39). Simultaneously, the power exchange between the microgrid system and the distribution network should be within the allowable range as given by Equation (40).

$$P_{Uncontro\_load}(t) + \sum_{i=1}^{M} P_{ac}(t) \cdot S_{ac}(t) + P_{sell}(t) = P_{PV}(t) + P_{buy}(t) \tag{39}$$

$$\begin{cases} 0 \le P_{sell}(t) \le P_{\max} \\ 0 \le P_{buy}(t) \le P_{\max} \end{cases} \tag{40}$$

2) Constraints of VESS

The constraints of VESS are explained in Section 3.1, which are shown in Equations (10) - (12). It should be noted that different air-conditioned households have different internal parameters due to the differences in building structure and occupants' activities etc. [42]. Therefore, Monte Carlo simulation is adopted to generate air-conditioned households with different parameters [43], which are further aggregated through an aggregator to form VESS.

3) Constraints of PV

In Section 3.3, the model of PV generation has been described in Equations (28)-(30). In addition, the limits of PV generation power should be satisfied as below:

$$0 \le P_{PV}(t) \le P_{PV}^{\max} \tag{41}$$

4.2. Second layer - BESS optimal sizing model

4.2.1 Objective

In this layer, to minimize system investment cost and operation cost, the model is formulated as a mixed-integer nonlinear programming (MINLP) problem to achieve the optimal sizing of BESS and the optimal energy resources dispatching. Simultaneously, the risk measure is given considering the uncertainties of PV generation and load. The model is formulated as follows:

$$\min C = \min\left(C_{BESS} + C_{O\&M}\right) \tag{42}$$

The relevant cost variables in Equation (42) are further formulated as follows:

$$C_{BESS} = A_{BESS}^{E} \cdot E_{BESS}^{rate} + A_{BESS}^{P} \cdot P_{BESS}^{rate} \tag{43}$$

$$C_{O\&M} = \min \sum_{T=1}^{T_{life}} \left[\left(C_O \cdot 365 + C_M\right) / K_{coef} \right] \tag{44}$$

Further, the relevant variables in Equation (44) are explained as follows:

$$C_O = \min \sum_{t=1}^{N} \left[\left(P_{buy}(t) \cdot C_{buy}(t) - P_{sell}(t) \cdot C_{sell}(t) \right) \cdot \tau \right] \tag{45}$$

$$C_M = A_{BESS\_M}^{E} \cdot E_{BESS}^{rate} + A_{BESS\_M}^{P} \cdot P_{BESS}^{rate} \tag{46}$$

$$K_{coef} = \frac{r'(1+r')^T}{(1+r')^T - 1} \tag{47}$$

$$r' = \frac{r-e}{1+e} \tag{48}$$

In addition, the net profit of BESS is formulated below:

$$C_{BESS\_back} = \sum_{T=1}^{T_{life}} \left[\left(C_{Arbi} \cdot 365 - C_M\right) / K_{coef} \right] - C_{BESS} \tag{49}$$

$$C_{Arbi} = \sum_{t=1}^{N} C_{arbi}(t) \tag{50}$$

$$C_{arbi}(t) = \begin{cases} \left[P_{BESS,Dis}(t) \cdot C_{buy}(t) - P_{BESS,Chr}(t) \cdot C_{buy}(t) \right] \cdot \tau \text{ , } t \in \text{Non-photovoltaic charging period to BESS} \\ \left[P_{BESS,Chr}(t) \cdot C_{buy}(t) - P_{BESS,Chr}(t) \cdot C_{sell}(t) \right] \cdot \tau \text{ , } t \in \text{Photovoltaic charging period to BESS} \end{cases} \tag{51}$$

Considering the uncertainties of photovoltaic power generation and electrical load, Equation (42) is formulated into a probabilistic version [40] which can reflect the trade-off between system costs and risks. Through the mean-variance Markowitz theory [44], a probabilistic version is formed as Equation (52). Backward

method [45] is used here to approximate the original scenarios to a smaller set to increase the computational efficiency.

$$\min\ E(C)+\omega\cdot\sigma_C \tag{52}$$

$$E(C)=\sum_{s=1}^{S}\mathrm{Pr}_s\cdot C_s \tag{53}$$

$$\sigma_C=\sqrt{E(C^2)-E^2(C)}=\sqrt{\sum_{s=1}^{S}\mathrm{Pr}_s\cdot C_s^2-\left(\sum_{s=1}^{S}\mathrm{Pr}_s\cdot C_s\right)^2} \tag{54}$$

Where $E(C)$ is the expected value of the system cost; σ_C is the standard deviation, $\omega\in[0,+\infty)$ is the weighting factor for the inclusion of risk, and the higher the value of ω, the more risk averse [40]. Pr_s and C_s are the probability and the system cost respectively under scenario s.

4.2.2 Constraints

1) Constraints of power balance

$$\begin{aligned}P_{Uncontro\_load}(t)+\sum_{i=1}^{M}P_{ac\_i}(t)\cdot S_{ac\_i}(t)+P_{BESS,Chr}(t)\cdot\mu_{BESS,Chr}(t)+P_{sell}(t)\cdot x_{sell}(t)\\ =P_{PV}(t)+P_{BESS,Dis}(t)\cdot\mu_{BESS,Dis}(t)+P_{buy}(t)\cdot x_{buy}(t)\end{aligned} \tag{55}$$

$$\begin{cases}0\le P_{sell}(t)\le P_{\max}\\ 0\le P_{buy}(t)\le P_{\max}\end{cases} \tag{56}$$

$$\begin{cases}\mu_{BESS,Chr}(t)+\mu_{BESS,Dis}(t)\le 1\\ \mu_{BESS,Chr}(t),\ \ \mu_{BESS,Dis}(t)\in\{0,1\}\end{cases} \tag{57}$$

$$\begin{cases}x_{sell}(t)+x_{buy}(t)\le 1\\ x_{sell}(t),x_{buy}(t)\in\{0,1\}\end{cases} \tag{58}$$

2) Constraints of VESS

In Sections 3.1 and 4.1, the constraints of VESS have been explained, which are Equations (11)-(12).

3) Constraints of BESS

In Section 3.2, the constraints of BESS have been explained, which are Equations (24)-(27).

4) Constraints of PV

The model and limit of PV generation have been described in Equations (28)-(30) and Equation (41), respectively.

5. Implementation of BESS Optimal Sizing Strategy

Based on the components modelling of smart microgrid system in Section 3 and mathematical model for the proposed strategy in Section 4, the detailed solution process of the proposed model is introduced in this section. The flow chart is shown in Fig. 3, which is composed of the first layer and the second layer.

The initial size of BESS is determined in the first layer, as followed by the specific steps:

- Step 1: Firstly, Block A is the data collection and input, including necessary meteorological data, the cost parameters of BESS, parameters of VESS, technical parameters of smart microgrid system, electricity price information and user demand, etc. In addition, PV generation can be calculated by Equations (28) – (30), and uncertainties of PV and load are considered by Equations (31) – (32);

- Step 2: In Block B, Monte Carlo simulation is applied to generate various air-conditioning household scenarios with different parameters, which are aggregated through an aggregator to form VESS as described in Section 3.1;
- Step 3: In Blocks C and D, the BESS initial sizing model given in Section 4.1 is presented. Taking 15 minutes as the time interval, MILP can be solved by MOSEK solver to obtain the intra-day load distribution and photovoltaic output in the smart microgrid;
- Step 4: In Block E, the initial size of BESS can be calculated by Equations (36) – (37).

Considering PV and load uncertainties, the optimal size of BESS and energy resources dispatching strategy are provided in the second layer. The detailed procedures are further given below:

- Step 5: Input/update rated power P_{BESS}^{rate} and rated capacity E_{BESS}^{rate} of BESS in Block F.
- Step 6: In Blocks G and H, considering the PV and load uncertainties, Monte Carlo simulation and the backward method are used to generate representative scenarios *S*.
- Step 7: In Block I, the BESS optimal sizing is determined for each scenarios *s* by differential evolution algorithm (DE) [46], and the value of objective function (Equation (42)) is recorded.
- Step 8: In Blocks K and L, the objective function value with risk measure is calculated by Equation (52) under the corresponding size of BESS. In the meanwhile, the system cost and optimal energy resources dispatching are decided.
- Step 9: As shown in Equation (59), the rated capacity of BESS is updated by iterative search method in Block M, which is returned to Block F. Until $E_{BESS}^{rate} > E_{BESS,\max}^{rate}$, the iteration cycle of rated capacity at this rated power is completed and the next iteration cycle of rated power is entered.

$$E_{BESS}^{rate} = E_{BESS}^{rate} + \delta_1 \tag{59}$$

- Step 10: As shown in Equations (60)-(62), the rated power of BESS is updated by the iterative search method in Blocks O, P and Q, which is returened to Block F. Until $P_{BESS}^{rate} > P_{BESS,\max}^{rate}$, the iteration of BESS size is completed and the next screening step is entered.

$$P_{BESS}^{rate} = P_{BESS}^{rate} + \delta_2 \tag{60}$$

$$E_{BESS}^{rate} = E_{BESS,Init}^{rate} \tag{61}$$

$$E_{BESS,\max}^{rate} = \gamma \cdot P_{BESS}^{rate} \tag{62}$$

- Step 11: In Block R and S, all size of BESS and system costs are exported, then the optimal size of BESS is screened out through comparing system costs.

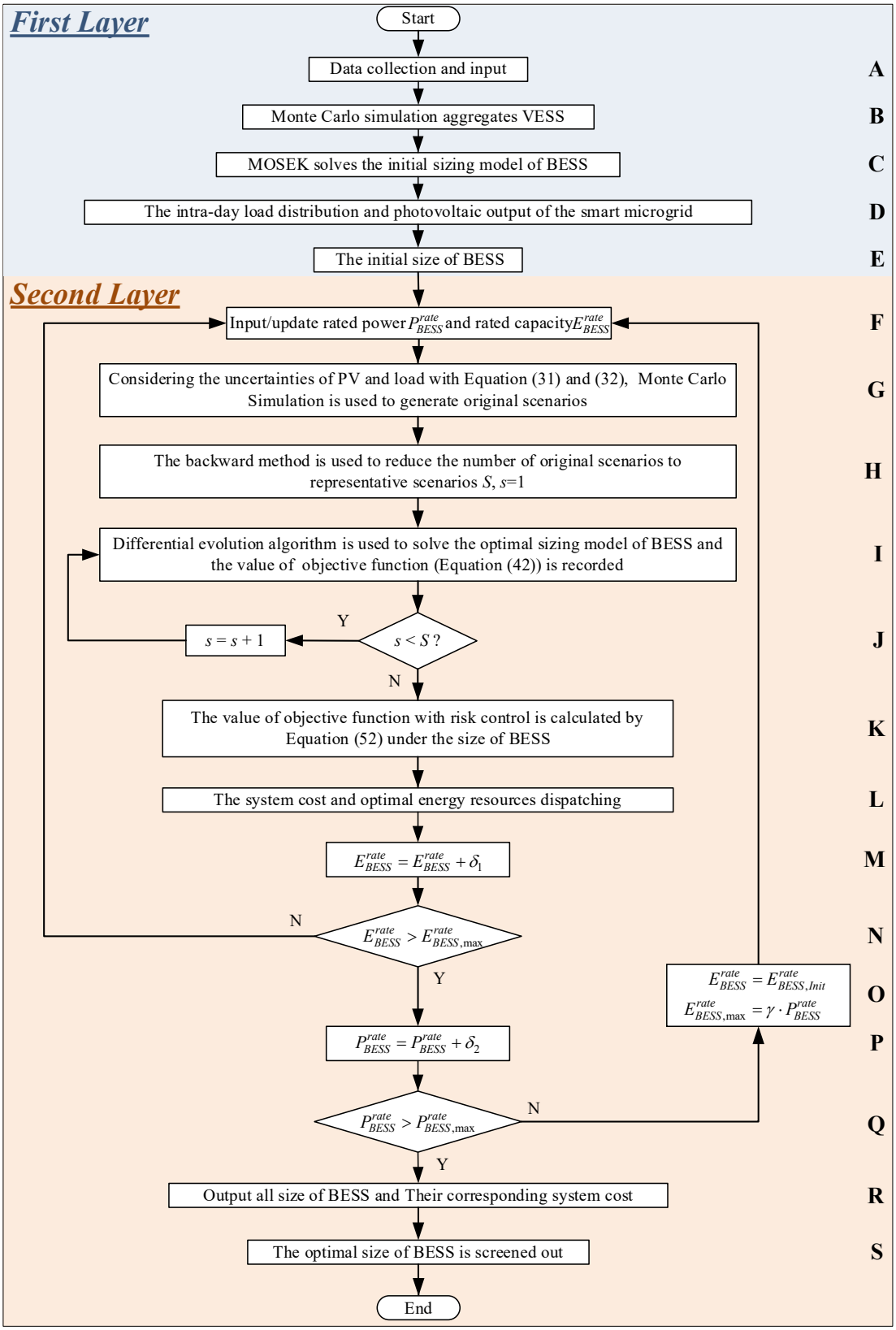

Fig. 3. Flow chart of optimal sizing of BESS

6. Case Studies

In order to verify the effectiveness of the proposed strategy for optimal sizing of BESS, this paper takes the microgrid system of a certain region as an example for case study. The tested microgrid system is shown in Fig. 4.

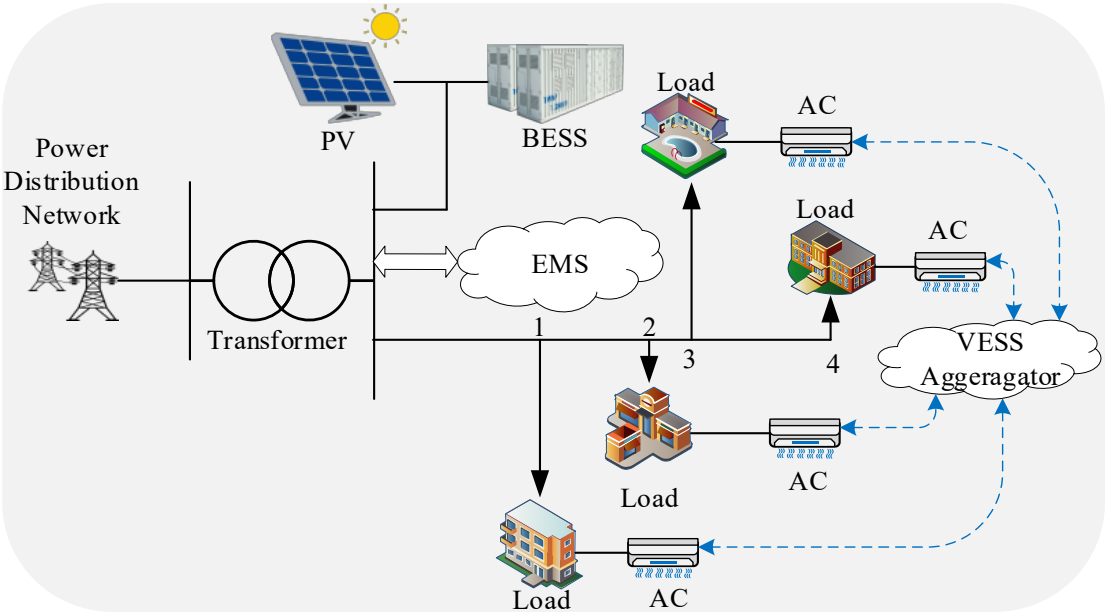

Fig. 4. The tested microgrid system

6.1. Setup

Based on the typical solar radiation and ambient temperature collected in Guangzhou, China [47], the PV output can be calculated by Equations (28) – (30). The load profile and photovoltaic profile in the tested microgrid system are given as Fig. 5. It should be noted that the typical summer temperature in this region is used in this paper. The time-of-use electricity price is considered, as shown in Fig. 6. It can be seen that the electricity purchase price from distribution grid at 9:15-12:00 and 19:15-22:00 is at the peak rates, 0:00-8:00 is at the off-peak rates, and the rest of the time is at the shoulder rates. The electricity selling price to the distribution grid is steady and lower than the electricity purchase price all day.

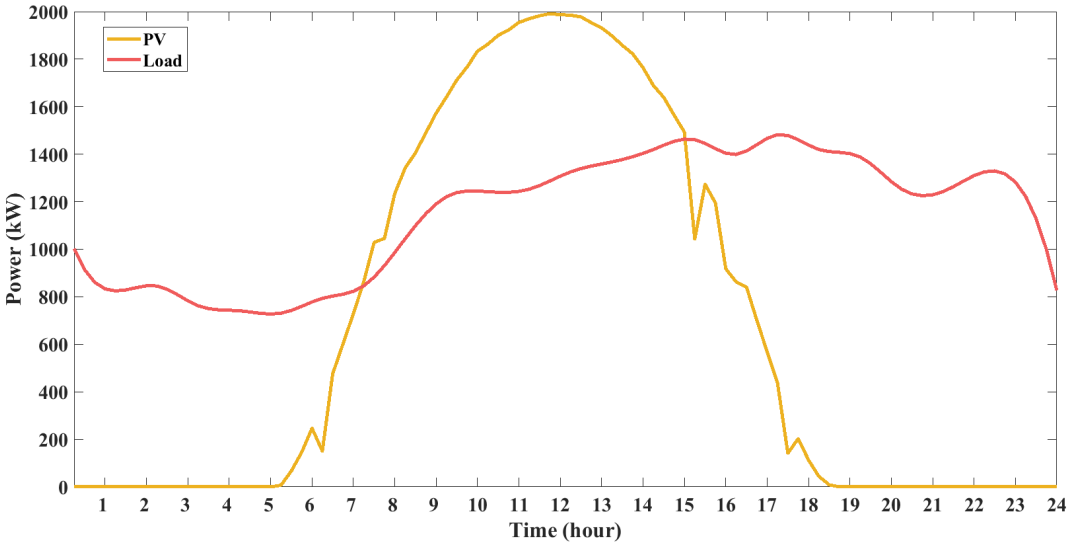

Fig. 5. Typical load and photovoltaic profile

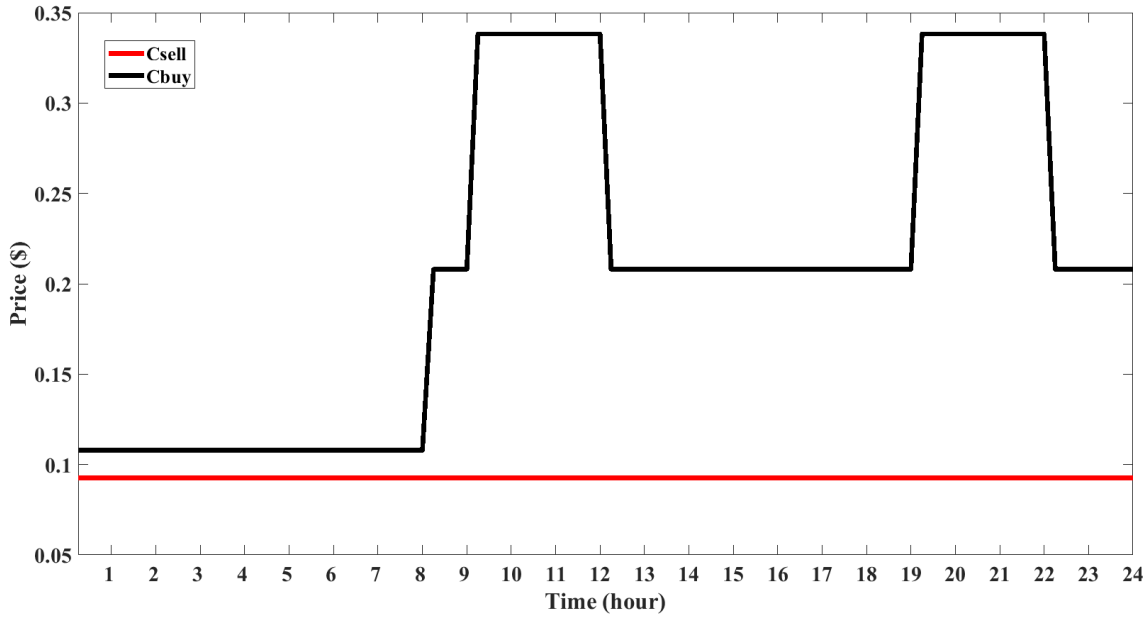

Fig. 6. Time-of-use electricity price

It is assumed that the aggregator in the microgrid system regulates 150 air-conditioned households, and the aggregator is further managed by the EMS. Monte Carlo simulation is employed here to generate various air-conditioned building scenarios with different parameters, which are further aggregated to form the virtual energy storage system. As described in Section 3.1, the equivalent thermal resistance of the VESS includes glass windows and walls, and the thermal capacitance of walls and the heat gain of the building. The parameters range of air-conditioned buildings is shown in Table 1.

The economic and technical analysis of the BESS in the grid is mainly affected by the profits, investment costs, operating costs, degradation and replacement costs [6]. Lithium ion battery has the advantages of high energy density, long calendar and cycle life, high charge/discharge efficiency, high reliability, low self-discharge rate, and satisfactory charging speed [4], which is suitable for the application scenario of microgrid system mentioned in this paper. The relevant parameters of BESS applied in the case study are shown in Table 2 [15].

Table 1 Relevant parameters of air-conditioned buildings for Monte Carlo simulation

Length of Building (m)	Width of Building (m)	Height of Building (m)	Width of Wall (m)
9-21	7-14	3-8	0.2-0.4
Number of Windows	Required Temperature (°C)	Rated Power for Air Conditioners (kW)	
3-9	23-27	1-7	

Table 2 Parameters of BESS [15]

A_{BESS}^{P} ($/kW)	A_{BESS}^{E} ($/kWh)	$A_{BESS\_M}^{E}$ ($/(kWh year))
300	250	7.5
$A_{BESS\_M}^{P}$ (($/(kWh year))	T_{life} (year)	$BSOC^{\min}$ / $BSOC^{\max}$ (%)
6	8	20/80
δ_{self_d} (%/day)	r (%)	e (%/year)
0.1	6	3.5

6.2. Sensitivity analysis

Considering the uncertainties of PV generation and load, a sensitivity analysis is performed to investigate the impact of uncertainties on BESS sizing. The corresponding results are shown in Fig. 7 and Fig. 8, where Fig. 7 denotes the sensitivity analysis of BESS rated power, and Fig. 8 denotes the sensitivity analysis of BESS rated capacity. As shown in the figures, the ratio of load is varying from 70% to 130%, while the PV generation ratio is varying from 40% to 100%.

It can be observed that from Fig. 7 and Fig. 8 that for the rated power of BESS, the PV generation change has little impact on it, while the load change has more influences on it. As the load amount gradually grows, the rated power of BESS gradually increases as well. In terms of the rated capacity of BESS, the change of PV generation has less impact than the change of load as well. It is worth noting that the rated capacity of BESS increases as the load grows. In other words, the investment cost of BESS can be reduced when the system load is decreased via utilizing demand response technologies.

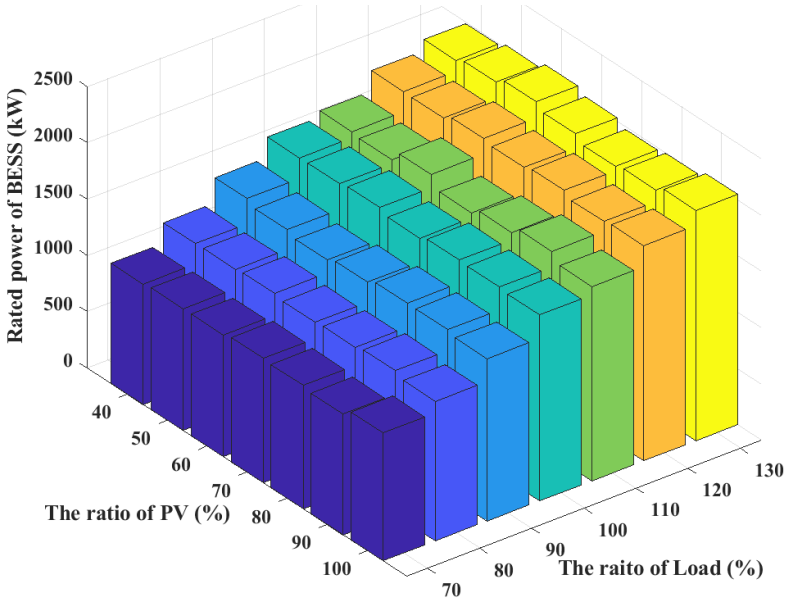

Fig. 7. Sensitivity of BESS rated power

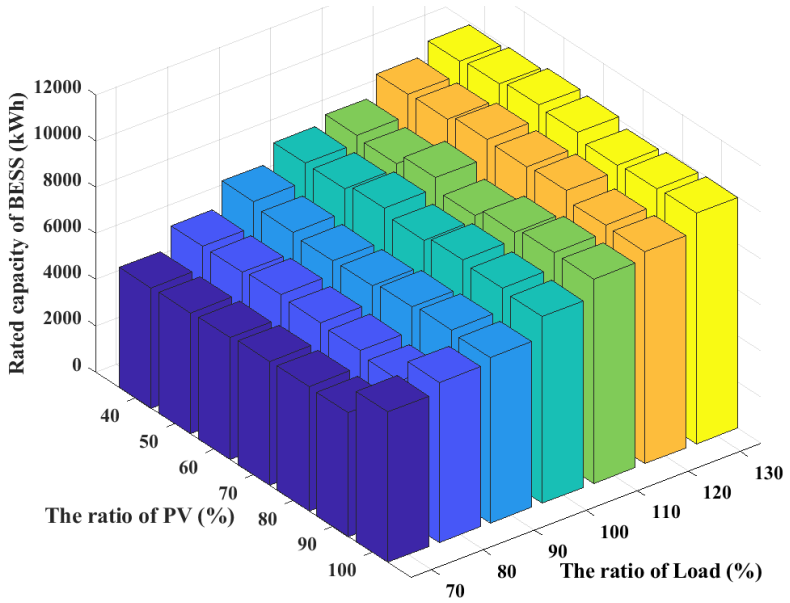

Fig. 8. Sensitivity of BESS rated capacity

6.3. Simulation results and discussion

In order to mitigate risks caused by system uncertainties, ω is chosen as 1.66 by sensitivity analysis [48] in this paper. Fig. 9 demonstrates the distribution of system cost during the entire lifecycle of BESS (8 years), which is overall shown as a normal distribution. The mean system cost and the standard deviation are \$ $2.64*10^7$ and \$ $7.53*10^6$, respectively. It can be found that the change in system cost is evident due to various uncertainties. Therefore, the risk of system cost variability is assessed during the optimal sizing of BESS. In this work, VaR(95%) is \$ $3.98*10^7$, which means that the maximum overall cost (loss) of the microgrid system is at the 95% confidence level during the 8 years.

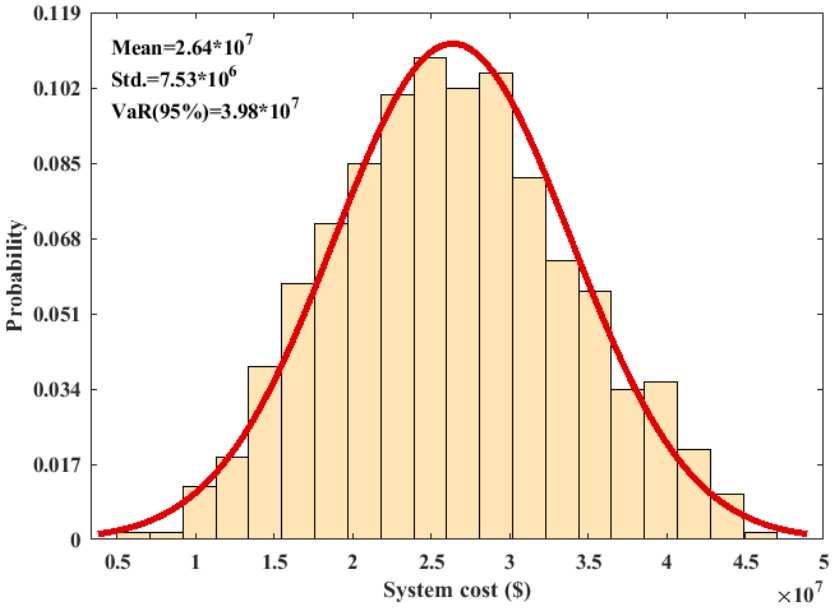

Fig. 9. Distribution of microgrid system cost during the entire lifecycle of BESS

The diagram of the relationship between the BESS size and the system cost is presented in Fig. 10, and the relationship between the size of BESS and the net profit of BESS is described in Fig. 11. As shown in Fig. 10, the system cost decreases with the increase of BESS size until it reaches saturation. In addition, BESS net profit increases to the saturation point as the size of BESS grows in the system as demonstrated by Fig.11. On the other hand, although the investment cost of BESS decreases with the reduction of size, the system is not able to profit from the installation of BESS when its size is too small. Therefore, the optimal size of BESS can be found while the system cost is minimal. It can be observed from Fig. 10, when the system cost is at minimal point, the optimal size of BESS is determined as rated power 1624.2 kW and rated capacity 8070.7 kWh.

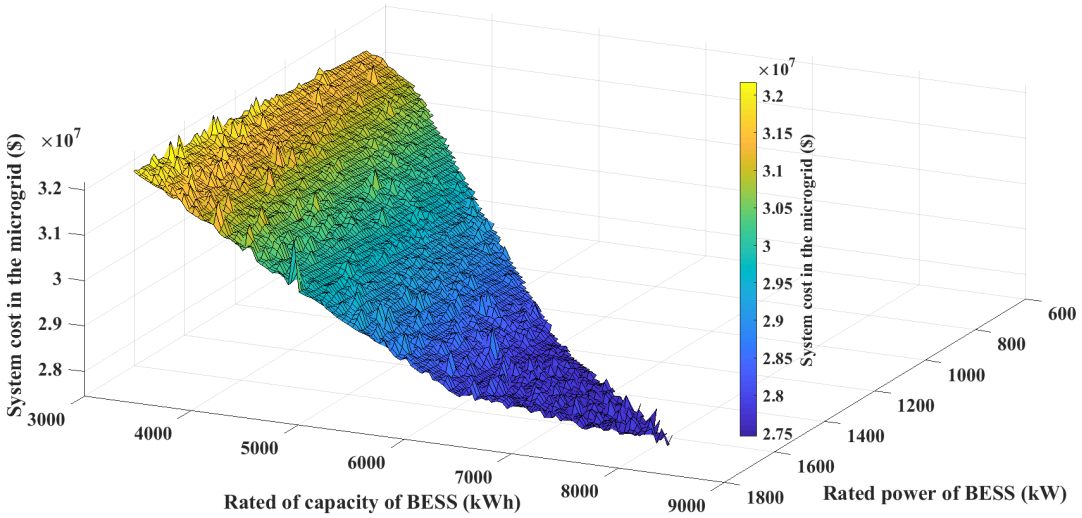

Fig. 10. Relationship between the size of BESS and the total cost of the microgrid

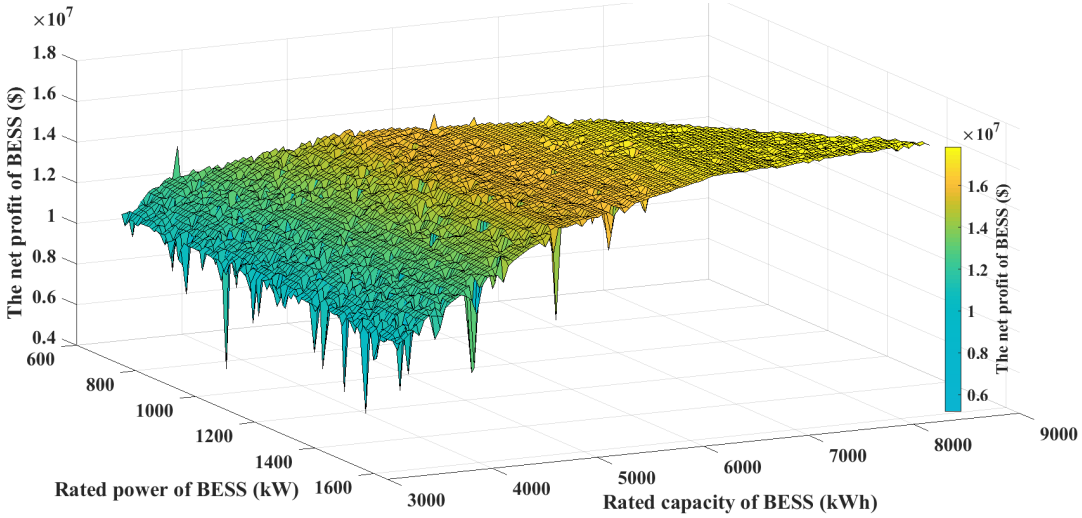

Fig. 11. Relationship between the size of BESS and the net profit of BESS

In order to verify the effectiveness of the proposed strategy when involving VESS, the corresponding results are described in Figs. 12 and 13. Fig. 12 shows the comparison of the operation status of an air conditioner with control and without control, which is selected stochastically in the aggregated VESS. The red line is the local typical ambient temperature, the blue line is the indoor air temperature, and the green line is the air conditioning dispatching status. Fig. 13 shows the operation status of VESS with and without control including VESS's power (positive value means charging power and negative value is discharging power) and VSOC. According to the ambient temperature in Fig. 12, it can be seen that VSOC decreases with the increase of the outdoor temperature from 7:00 to 9:00, and VSOC with control drops much faster than VSOC without control mode. In order to meet the users thermal comfort requirements, VSOC with control changes with time and stays at a relatively low position (around 35%) from 10:00 to 18:00, but VSOC without control has less temporal change and is at a relatively high position (around 68%). From 19:00 to 21:00, VSOC with control increases with the drop of ambient temperature, while VSOC without control mode is the opposite. The different energy dispatching results between VESS with control and VESS without control is due to VESS with control is influenced by the combination of electricity energy expenditure and required thermal comfort of users, but VESS without control is only affected by the users' required thermal settings. In addition, regardless of whether VESS is in control mode or not, it can maintain a relatively stable state due to the low and stable ambient temperature from 21:00 to 7:00.

Furthermore, it should also be noted that the change of VSOC with control mode is quite intense when the electricity price is during peak periods from 9:15 to 12:00.

It can be observed that VESS changes are largely affected by the ambient temperature. Compared with BESS, VESS has fast energy dissipation characteristics and allows deep discharge. Similar to battery storage systems, VESS can make use of its own thermal buffer characteristics to achieve energy saving and emission reduction. With the accurate modelling of VESS, end users' thermal comfort is guaranteed. Furthermore, VESS in control mode can improve energy efficiency and has more energy-saving and emission-reduction than VESS without control under the same user comfort requirement. In other words, the system load can be reduced due to the thermal buffer involvement from VESS. Therefore, based on the sensitivity study at Section 6.2, it can be concluded that the BESS investment cost is further reduced through the involvement of VESS.

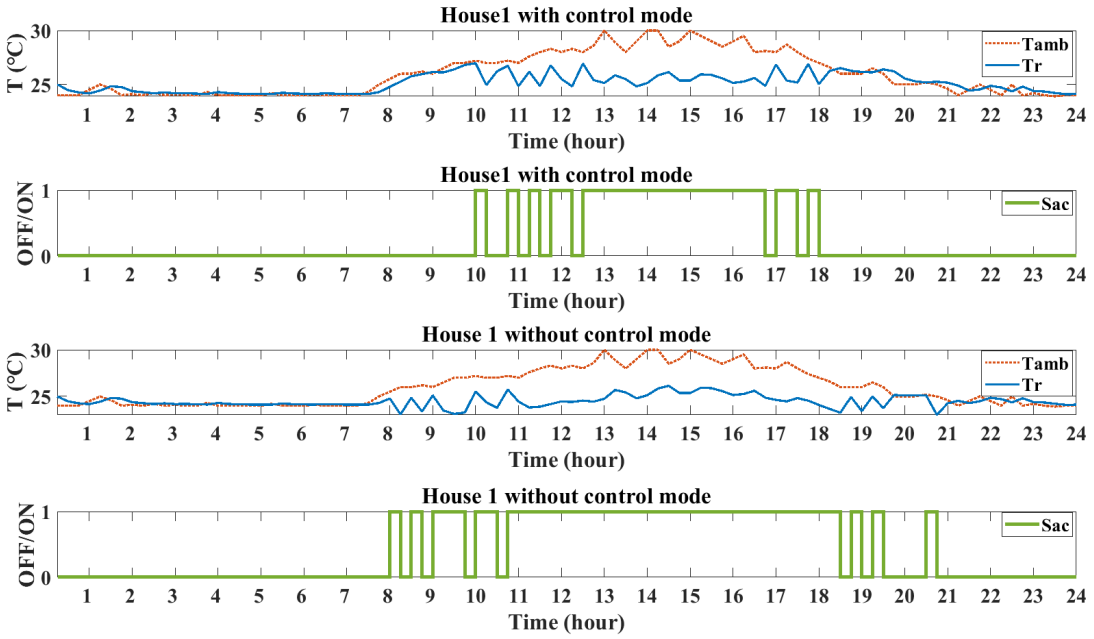

Fig. 12. Optimal and random operation of the air-conditioned building

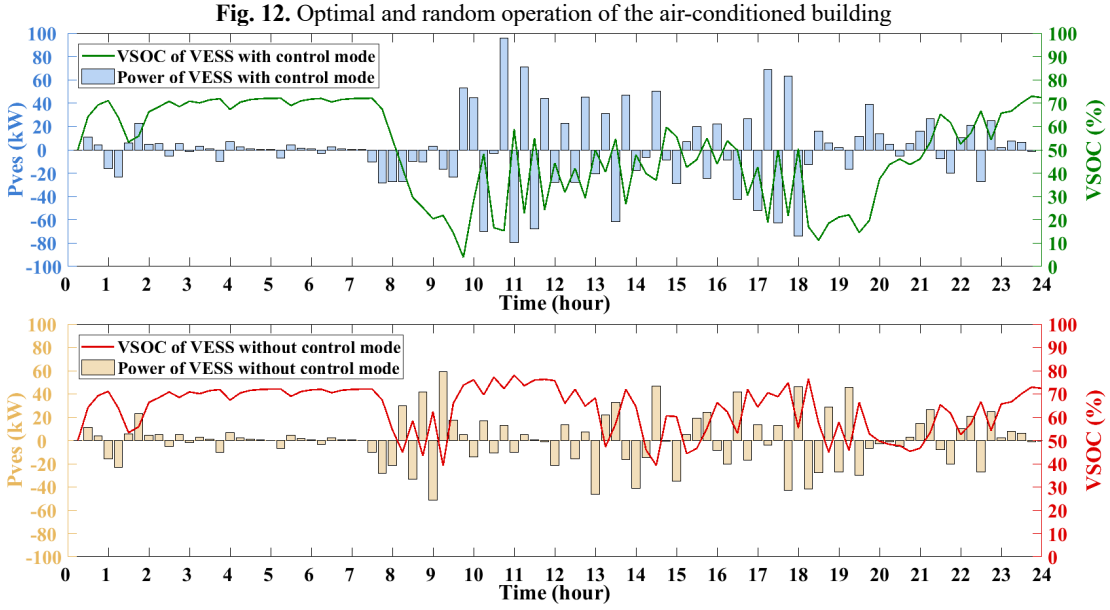

Fig. 13. Operation status of VESS with and without control mode

The charging/discharging power and BSOC of BESS are denoted in Fig. 14. It can be observed that BESS is charged from the distribution grid or PV system when the electricity purchase price from distribution grid is at the lowest rates level or there is surplus output from photovoltaic power generation. On the contrary, BESS is

discharged to supply the load during the peak electricity purchase price periods, and the remaining capacity of BESS is discharged within system constraints during the shoulder electricity price periods. Hence, electricity price arbitrage can be achieved by BESS through selected charging/discharging periods. In addition, as the energy buffer unit, BESS configured in the framework is sufficient to achieve the on-site consumption of PV generation and alleviate the uncertainty of high PV penetration to keep the system stable operation.

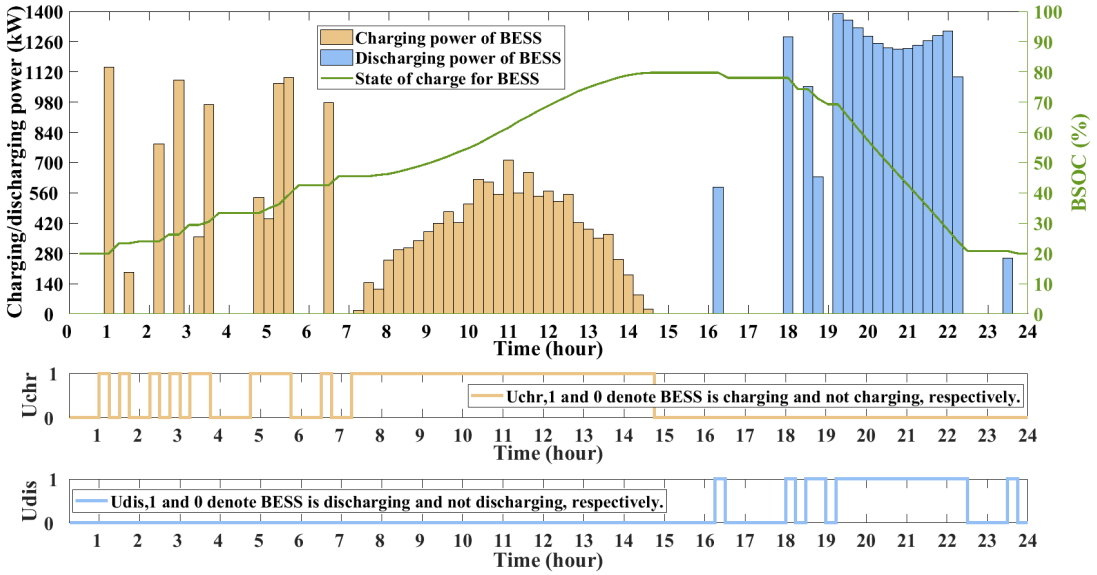

Fig. 14. Charging/discharging power and BSOC of BESS

The electricity consumption of smart microgrid system from external distribution network is depicted in Fig. 15. As depicted, the microgrid system only consumes power from the distribution network system during the off-peak or shoulder electricity price periods. It should also be noted that the amount of electricity sold from the microgrid system to the distribution network system is 0 throughout the day, due to the surplus PV generation is consumed directly by the charging of BESS and the electricity selling price to distribution grid always is lower than the electricity purchase price. Besides, when there is surplus output from photovoltaic power generation or the electricity purchase price from distribution grid is at the lowest level, the microgrid system work in islanded modes until the internal energy supply including PV and BESS are insufficient. In summary, through analyzing the simulation results, it can be found that energy resources (i.e. PV, BESS and VESS) can be dispatched optimally through the proposed strategy to minimize system operation cost and improve energy efficiency while meeting various system constraints.

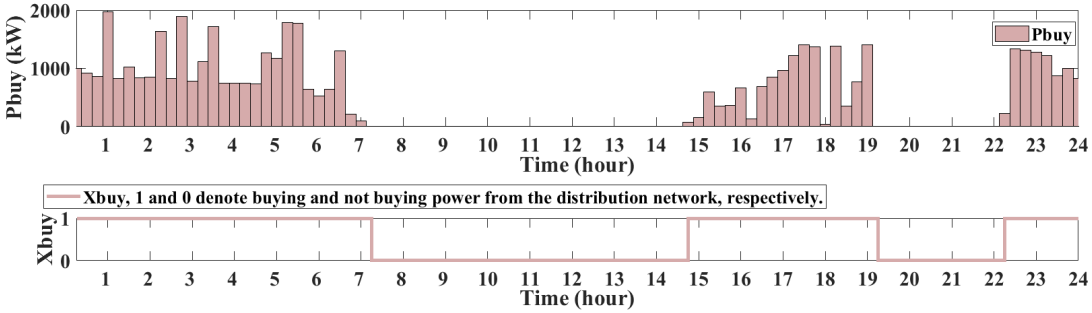

Fig. 15. Electricity purchasing status of smart microgrid system

7. Conclusion

This paper proposes an innovative BESS optimal sizing strategy considering dispatch of VESS in the smart microgrid with high photovoltaic penetration. The proposed model is composed of two layers. In the first layer, VESS modelling and aggregation are established, and the initial size of BESS is determined by considering VESS participation in demand response program. In the second layer, the optimal sizing of BESS and the optimal energy resources dispatching strategy are studied. In the meanwhile, the risk of system cost variability is assessed by the mean-variance Markowitz theory. The simulation results demonstrate that the proposed strategy can achieve optimal sizing of BESS, minimize system cost, and mitigate the impact of uncertainties. Compared with previous research, this work is advantageous in, 1) employing a more accurate two-parameter thermal model with internal heating taken into account to establish the VESS model; 2) determining the optimal sizing of BESS with the involvement of VESS and high PV penetration; 3) analyzing the system cost risks in detail by incorporating mean-variance Markowitz theory based risk factors.

Acknowledgments

This work is sponsored by the Department of Finance and Education of Guangdong Province 2016 [202]: Key Discipline Construction Program, China; the Education Department of Guangdong Province: New and Integrated Energy System Theory and Technology Research Group [Project Number 2016KCXTD022]; and Brunel University London BRIEF Funding, UK.

References

[1] IRENA. Global Energy Transformation: A roadmap to 2050, Tech. rep., IRENA, Abu Dhabi; 2018. < http://www.irena.org/publications/2018/Apr/Global-Energy-Transition-A-Roadmap-to-2050 >.

[2] H. Hao, D. Wu, J. Lian and T. Yang, "Optimal coordination of building loads and energy storage for power grid and end user services," *IEEE Transactions on Smart Grid*, vol. 9, no. 5, pp. 4335-4345, September 2018.

[3] C.S. Lai, Y. Jia, L.L. Lai, Z. Xu, M.D. McCulloch and K.P. Wong, "A comprehensive review on large-scale photovoltaic system with applications of electrical energy storage," *Renewable and Sustainable Energy Reviews*, vol. 78, pp. 439-451, October 2017.

[4] M. Killer, M. Farrokhseresht and N.G. Paterakis, "Implementation of large-scale Li-ion battery energy storage systems within the EMEA region," *Applied Energy*, vol. 260, pp. 114166, February 2020.

[5] Y. Zheng, D.J. Hill and Z.Y. Dong, "Multi-agent optimal allocation of energy storage systems in distribution systems," *IEEE Transactions on Sustainable Energy*, vol. 8, no. 4, pp. 1715-1725, October 2017.

[6] C.S. Lai, G. Locatelli, A. Pimm, Y. Tao, X. Li and L.L. Lai, "A financial model for lithium-ion storage in a photovoltaic and biogas energy system," *Applied Energy*, vol. 251, pp. 113179, October 2019.

[7] L. Zhou, Y. Zhang, X. Lin, C. Li, Z. Cai and P. Yang, "Optimal sizing of PV and BESS for a smart household considering different price mechanisms," *IEEE Access*, vol. 6, pp. 41050-41059, June 2018.

[8] Z. Liu, Y. Chen, R. Zhuo and H. Jia. "Energy storage capacity optimization for autonomy microgrid considering CHP and EV scheduling," *Applied Energy*, vol. 210, pp. 1113-1125, January 2018.

[9] M.R. Jannesar, A. Sedighi, M. Savaghebi and J.M. Guerrero, "Optimal placement, sizing, and daily charge/discharge of battery energy storage in low voltage distribution network with high photovoltaic penetration," *Applied Energy*, vol. 226, pp. 957-966, September 2018.

[10] R. Hemmati and H. Saboori, "Stochastic optimal battery storage sizing and scheduling in home energy management systems equipped with solar photovoltaic panels," *Energy and Buildings*, vol. 152, pp. 290-300, October 2017.

[11] J.M. Lujano-Rojas, J.A. Domínguez-Navarro, J.M. Yusta, G.J. Osório, M. Lotfi and J.P.S. Catalão, "Massive integration of wind power at distribution level supported by battery energy storage systems," *2019 IEEE Milan Power Tech*, Milan, Italy, pp. 1-6, June 2019.

[12] C.S. Lai and M.D. McCulloch, "Sizing of stand-alone solar PV and storage system with anaerobic digestion biogas power plants," *IEEE Transactions on Industrial Electronics*, vol. 64, no. 3, pp. 2112-2121, March 2017.

[13] H. Bludszuweit and J.A. Dominguez-Navarro, "A probabilistic method for energy storage sizing based on wind power forecast uncertainty," *IEEE Transactions on Power Systems*, vol. 26, no. 3, pp. 1651-1658, August 2011.

[14] M. Ban, D. Guo, J. Yu and M. Shahidehpour, "Optimal sizing of PV and battery-based energy storage in an off-grid nanogrid supplying batteries to a battery swapping station," *Journal of Modern Power Systems and Clean Energy*, vol. 7, no. 2, pp. 309-320, March 2019.

[15] D. L. Rodrigues, X. Ye, X. Xia and B. Zhu, "Battery energy storage sizing optimisation for different ownership structures in a peer-to-peer energy sharing community," *Applied Energy*, vol. 262, pp. 114498, March 2020.

[16] T. Terlouw, T. AlSkaif, C. Bauer and W. van Sark, "Optimal energy management in all-electric residential energy systems with heat and electricity storage," *Applied Energy*, vol. 254, pp. 113580, November 2019.

[17] S. van der Stelt, T. AlSkaif and W. van Sarik, "Techno-economic analysis of household and community energy storage for residential prosumers with smart appliances," *Applied Energy*, vol. 209, pp. 266-276, January 2018.

[18] S. Zhong, J. Qiu, L. Sun, Y. Liu, C. Zhang and G. Wang, "Coordinated planning of distributed WT, shared BESS and individual VESS using a two-stage approach," *International Journal of Electrical Power & Energy Systems*, vol. 114, pp. 105380, January 2020.

[19] C. Perfumo, J.H. Braslavsky and J.K. Ward, "Model-based estimation of energy savings in load control events for thermostatically controlled loads," *IEEE Transactions on Smart Grid*, vol. 5, no. 3, pp. 1410-1420, May 2014.

[20] M. Ma, X. Ma, W. Cai and W. Cai, "Low carbon roadmap of residential building sector in China: Historical mitigation and prospective peak," *Applied Energy*, vol. 273, pp. 115247, Sep. 2020.

[21] L. Chen, W. Cai and M. Ma, "Decoupling or delusion? Mapping carbon emission per capita based on the human development index in Southwest China," *Science of The Environment*, vol. 741, pp. 138722, Nov. 2020.

[22] M. Ma and W. Cai, "Towards low carbon pathway of the commercial building sector for 2070: Lessons from China," *Applied Energy Symposium 2020: Low Carbon Cities and Urban Energy Systems (CUE2020)*, Virtual Symposium, October 2020. DOI: 10.13140/RG.2.2.11456.15364.

[23] N.S. Raman and P. Barooah, "On the round-trip efficiency of an HVAC-based virtual battery," *IEEE Transactions on Smart Grid*, vol. 11, no. 1, pp. 403-410, January 2020.

[24] C. Xie, D. Wang, C.S. Lai, R. Wu, J. Huang and L.L. Lai, "Optimal sizing of battery energy storage systems in smart microgrid with air-conditioning resources," *2020 IEEE International Smart Cities Conference (ISC2)*, Virtual Conference, September/October 2020.

[25] H. Wang, K. Meng, F. Luo, Z.Y. Dong, G. Verbič, Z. Xu and K.P. Wong, "Demand response through smart home energy management using thermal inertia," *2013 Australasian Universities Power Engineering Conference (AUPEC)*, Hobart, TAS, pp. 1-6, September 2013.

[26] X. Jin, Y. Mu, H. Jia, J. Wu, T. Jiang and X. Yu, "Dynamic economic dispatch of a hybrid energy microgrid considering building based virtual energy storage system," *Applied Energy*, vol. 194, pp. 386-398, May 2017.

[27] X. Zhu, J. Yang, Y. Liu, C. Liu, B. Miao and L. Chen, "Optimal scheduling method for a regional integrated energy system considering joint virtual energy storage," *IEEE Access*, vol. 7, pp. 138260-138272, September 2019.

[28] M. Cheng, S.S. Sami and J. Wu, "Benefits of using virtual energy storage system for power system frequency response," *Applied Energy*, vol. 194, pp. 376-385, May 2017.

[29] Y. Lin, P. Barooah, S. Meyn and T. Middelkoop, "Experimental evaluation of frequency regulation from commercial building HVAC systems," *IEEE Transactions on Smart Grid*, vol. 6, no. 2, pp. 776-783, March 2015.

[30] D. Wang, K. Meng, X. Gao, J. Qiu, L.L. Lai and Z.Y. Dong, "Coordinated dispatch of virtual energy storage systems in LV grids for voltage regulation," *IEEE Transactions on Industrial Informatics*, vol. 14, no. 6, pp. 2452-2462, June 2018.

[31] X. Jin, J. Wu, Y. Mu, M. Wang, X. Xu and H. Jia, "Hierarchical microgrid energy management in an office building," Applied Energy, vol. 208, pp. 480-494, December 2017.

[32] T. Hubert and S. Grijalva, "Modeling for residential electricity optimization in dynamic pricing environments," *IEEE Transactions on Smart Grid*, vol. 3, no. 4, pp. 2224-2231, December 2012.
[33] Y. Ji, Q. Xu, K. Luan and B. Yang, "Virtual energy storage model of air conditioning loads for providing regulation service," *Energy Reports*, vol. 6, pp. 627-632, February 2020.
[34] D. Wang, R. Wu, X. Li, C.S. Lai, X. Wu, J. Wei, Y. Xu, W. Wu and L.L. Lai, "Two-stage optimal scheduling of air conditioning resources with high photovoltaic penetrations," *Journal of Cleaner Production*, vol. 241, pp. 118407, December 2019.
[35] Z. Magyar, L. Garbai and A. Jasper, "Risk-based determination of heat demand for central and district heating by a probability theory approach," *Energy and Buildings*, vol. 110, pp. 387-395, January 2016.
[36] L. Yang and Y. Li, "Cooling load reduction by using thermal mass and night ventilation," *Energy and Buildings*, vol. 40, pp. 2052-2058, 2008.
[37] R. Bălan, J. Cooper, K.M. Chao, S. Stan, R. Donca, "Parameter identification and model based predictive control of temperature inside a house," *Energy and Buildings*, vol. 43, pp. 748-758, February 2011.
[38] X. Wu, X. Hu, X. Yin, C. Zhang and S. Qian, "Optimal battery sizing of smart home via convex programming," *Energy*, vol. 140, pp. 444-453, December 2017.
[39] H. Tazvinga, X. Xia and J. Zhang, "Minimum cost solution of photovoltaic–diesel–battery hybrid power systems for remote consumers," *Solar Energy*, vol. 96, pp. 292-299, October 2013.
[40] D. Wang, J. Qiu, L. Reedman, K. Meng and L.L. Lai, "Two-stage energy management for networked microgrids with high renewable penetration," *Applied Energy*, vol. 226, pp. 39-48, September 2018.
[41] Y. Zheng, J. Zhao, Y. Song, F. Luo, K. Meng, J. Qiu, and D.J. Hill, "Optimal operation of battery energy storage system considering distribution system uncertainty," *IEEE Transactions on Sustainable Energy*, vol. 9, no. 3, pp. 1051-1060, July 2018.
[42] D. Wang, H. Jia, C. Wang, N. Lu, M. Fan, W. Miao and Z. Liu, "Performance evaluation of controlling thermostatically controlled appliances as virtual generators using comfort-constrained state-queueing models," *IET Generation, Transmission & Distribution*, vol. 8, no. 4, pp. 591–599, April 2014.
[43] T. Balezentis and D. Streimikiene, "Multi-criteria ranking of energy generation scenarios with Monte Carlo simulation," *Applied Energy*, vol. 185, pp.862-871, January 2017.
[44] H. Markowitz. Portfolio selection: efficient diversification of investments. NewHaven, CT: Yale University Press; 1959.
[45] Y. Xu, Z.Y. Dong, R. Zhang and D.J. Hill, "Multi-timescale coordinated voltage/Var control of high renewable-penetrated distribution systems," *IEEE Transactions on Power Systems*, vol. 32, no. 6, pp. 4398-4408, November 2017.
[46] R. Storn and K. Price, "Differential evolution – A simple and efficient heuristic for global optimization over continuous spaces," *Journal of Global Optimization*, vol. 11, pp.341–359, December 1997.
[47] China Meteorological Data Service Center Website. Available: http://data.cma.cn. (Visited on 8 May 2020)
[48] J. Qiu, K. Meng, Y. Zheng and Z.Y. Dong, "Optimal scheduling of distributed energy resources as a virtual power plant in a transactive energy framework," *IET Generation, Transmission & Distribution*, vol. 11, no. 13, pp. 3417-3427, September 2017.